Experimental studies and simple numerical modeling of underwater electric discharges

Thanasi Frost ; Bucur M. Novac; Peter Senior; Laurent Pecastaing; Thierry Reess

Check for updates

View Online

Export Citation

25 April 2024 03:58:58

Experimental studies and simple numerical modeling of underwater electric discharges

Thanasi Frost,[1,a] Bucur M. Novac,[1,b] Peter Senior,[1] Laurent Pecastaing,[2] and Thierry Reess[2]

[1]*Wolfson School of Mechanical, Electrical and Manufacturing Engineering, Loughborough University, Loughborough, Leicestershire LE11 3TU, United Kingdom*

[2]*Laboratoire des Sciences de l'Ingénieur Appliquées à la Mécanique et au Génie Electrique—Fédération Institut Pluridisciplinaire de Recherche Appliquée, Université de Pau et des Pays de l'Adour/E2S UPPA, 64000 Pau, France*

ABSTRACT:

At present, underwater electric pulsed discharges are used in a wide range of modern applications. During the development of a system for generating underwater acoustic pressure pulses, a numerical model is an essential tool for guiding the design and interpreting the data. Developing a complex one-dimensional numerical code, like those presented in the literature, requires a substantial dedicated effort. Unfortunately, previous work trying to use simple and elegant theoretical models developed many decades ago reported a fundamental issue, apparently related to the input data. The present work performs a detailed analysis of the real meaning of the voltage measured across an underwater discharge and clarifies the correct way the power input to a simple two-phase model should be calculated. Based on accurate measurements, a phenomenological methodology to obtain the input data is demonstrated, with theoretical predictions obtained from the simple two-phase model being successfully compared with the experimental evidence obtained from both the present work as well as from other reliable data presented in the literature. © 2022 Author(s). All article content, except where otherwise noted, is licensed under a Creative Commons Attribution (CC BY) license (http://creativecommons.org/licenses/by/4.0/). https://doi.org/10.1121/10.0010288

I. INTRODUCTION

Underwater electric discharges have been used for decades in a large number of industrial applications including: underwater welding and electro-hydraulic forming,[1] shockwave generation for industrial sludge treatment, removal of foreign deposits from pipe walls or materials fragmentation, separation, reduction, and recycling,[2–4] for mining applications such as blasting[5] and drilling,[6] for demolition,[6] wastewater treatment,[7] sterilization,[8] bio-fouling control,[9] removal of algae,[10] underwater ultrasound sources,[11,12] as well as special bio-medical applications. A number of these applications are well described in a book dedicated to the pulsed electric breakdown of liquid phenomena.[13] Although the examples cited above are from the 1990s, this technology has been widely in use since the 1950s for marine seismic exploration and still it is in some specific cases.

There are two known breakdown mechanisms. *Supersonic*, in which the phenomenon is initiated by the formation of streamers created by a high voltage, fast rise time pulse with a nonhomogeneous field between a charged point and a ground plane. A resultant "electron avalanche" at the electrode point leads to the formation of streamers moving faster than the speed of sound in water. In the *subsonic* discharge, the streamer

mechanism is replaced by a thermal mechanism, where the plasma created is moving slower than the speed of sound in water. A slower rise time allows for conduction currents in the water, causing the water surrounding the electrodes to heat up and evaporate. This causes the formation of gas between the electrodes, which becomes the route for breakdown. This paper will focus on the latter phenomenon.

Recently, a research program has been initiated at Loughborough University in collaboration with Pau University to develop a repetitive underwater electric discharge system for an industrial application, requiring good high-pressure reproducibility. As also recently demonstrated experimentally, however, subsonic underwater discharges cannot generate highly reproducible pressure impulses.[14] Efforts to improve the reproducibility by shaping the electrodes to generate and control the inter-electrode electric field distribution were not successful.[14] In such conditions, one way to obtain reproducible phenomena is by using a very thin exploding wire as a *trigger* for the discharge, here termed "*pilot*," mounted between the two underwater electrodes. This technique, suggested in Ref. 15 was first demonstrated in Ref. 16 and later by others[17] to generate a well-defined cylindrical plasma discharge between the two discharge electrodes. The first aim of the present work is therefore to experimentally study all the details of the exploding wire triggered plasma discharge phenomena, using a relatively low-voltage capacitor bank that discharges considerably slower than those previously presented in the literature. The second and main aim is to determine the less time-consuming and most

a)Electronic mail: t.frost2@lboro.ac.uk

b)Also at: Laboratoire des Sciences de l'Ingénieur Appliquées à la Mécanique et au Génie Electrique—Fédération Institut Pluridisciplinaire de Recherche Appliquée, Université de Pau et des Pays de l'Adour/E2S UPPA, 64000 Pau, France.

straightforward way to obtain a theoretical *estimate* for the most important measurable characteristics of the complex underwater discharge phenomena such as the pressure impulse generated, and the dynamics of the bubble formed during the discharge. Such a simple model will then be used in guiding the design through the multi-parameter space of an optimized and repetitive system for industrial applications.

The structure of the paper is as follows. Section II presents a short overview of the main literature dedicated to numerical modeling underwater discharges. A critical analysis of the models available suggests conclusions that require experimental confirmation. Section III describes the hardware used in the present experimental studies: the power source, together with the practical arrangement at the laboratory water tank, as well as the complete set of diagnostic instrumentation. Section IV presents the main experimental findings compared with the theoretical predictions. The final part includes conclusions, along with a plan of future developments.

II. BRIEF OVERVIEW OF THE NUMERICAL MODELS RELATED TO UNDERWATER DISCHARGE AND THEIR ANALYSIS

A. Brief overview of numerical models

The theoretical models presented in the literature can be categorized as complex and simple.

The most detailed include one-dimensional (1D) models such as those in Refs. 18, 19, and 20 as well as *simplified* 1D models, such as those in Refs. 21 and 22. The simplified 1D models consider the pressure, temperature and mass density homogeneously distributed inside the plasma volume. It is, however, important to note that, according to Ref. 19 and as demonstrated in this work, simplified 1D models using proper electrical conductivity data can provide results extremely close to those generated by detailed 1D modeling.

A particular class of complex numerical models are based on finite-difference integration schemes, for example,[23] but such models are no longer used.

On the other hand, the simplest models, such as those presented in Refs. 24 and 25, are of no use for designing new systems for industrial applications, as they only describe the bubble dynamics.

A relatively simple but extremely elegant class of models, which does not consider all phenomena, is based on a pioneering theoretical work published in the late 1960s.[26] During the following years, this original theoretical approach was improved, massively extended and published as part of a monography dedicated to the hydrodynamical description of underwater electrical discharges, a work that still remains a valuable reference.[15] More recently many authors, for example, Refs. 11, 27, and 28, based their theoretical analysis on these simple models. Unfortunately, the main problem highlighted in Ref. 28 is that using the models described in Ref. 15, a good agreement with experimental data could only be achieved for discharges performed at a very low energy, i.e., for a total energy stored in the capacitor bank of less than 200 J.[28] For much higher energies, as in

Ref. 27, it was not possible to get an agreement with experimental data. The method used in Ref. 27 was to first determine experimentally a value for the "plasma resistance" and then use this value to calculate the input energy required by the model to match the experimental data. For obtaining a good agreement with the experimental evidence however, the experimentally obtained "plasma resistance" was required to be divided by a factor close to 3.

B. Analysis

Apparently, there is an important misunderstanding in the literature: the experimental determination of the plasma resistance, as presented, for example, in Refs. 20 and 27, is not possible. To understand the reason why the plasma resistance of an underwater discharge cannot be directly measured or straightforwardly inferred from experimental data, one must consider a very well understood system: an antenna, used to radiate electromagnetic energy.

According to the antenna textbook,[29] the impedance Z_A presented by an antenna or electromagnetic source at its input terminals, or the ratio of the voltage to current at the pair of input terminals, is given by $Z_A = R_A + jX_A$, where R_A is the antenna resistance and X_A is the antenna reactance. In turn, the electromagnetic source (antenna) resistance consists of two terms $R_A = R_r + R_J$, where R_r is the radiation resistance and R_J is the loss resistance. In other words, the first term is related to the energy lost by electromagnetic radiation, while the second term is the Joule energy lost by heating the antenna conductors.

In a similar way, for an underwater discharge, the ratio of voltage to current at the pair of input electrodes represents the underwater load (acoustic source) impedance Z_L, which can be written as

$$Z_L = R_L + jX_L, \tag{1}$$

where R_L is the load (discharge) resistance and X_L is the load inductive reactance. However, the underwater load (acoustic source) resistance has more terms than the resistance of the electromagnetic source:

$$R_L = R_{PL} + R_{SW} + R_H + R_E + R_O \tag{2}$$

with each term related to an energy absorption mechanism. The term R_{PL} is the plasma resistance related to the heating of the plasma column, R_{SW} is related to the energy lost by generating shock waves, R_H is related to the energy lost by heating water vapor (i.e., generating steam), R_E is related to the energy lost by electromagnetic radiation and finally R_O is related to the energy lost by other mechanisms, such as electrode erosion (detailed below). All terms of Eq. (2) are time dependent.

When the voltage V_L across the discharge electrodes and the current I flowing through the discharge are both measured during a test, Ohm's law provides the impedance,

$$Z_L(t) = \frac{V_L(t)}{I(t)}. \tag{3}$$

By measuring the current time rate-of-change dI/dt and using a technique presented below, the resistive part R_L of the impedance can indeed be obtained. But that is all that can be done: there is no direct way to obtain the fraction of this resistance representing the plasma resistance. Therefore, the resistance measured and used in the calculations in the various publications (for example, in Refs. 20 and 27) represents the overall resistance of the discharge, i.e., the load resistance R_L, rather than the plasma resistance R_{PL}. The time-dependent plasma resistance can only be calculated based on a 1D model as

$$R_{PL}(t) = \frac{l}{\sigma(t) \cdot \pi \cdot a(t)^2}, \quad (4)$$

where $\sigma(t)$ is the time dependent plasma conductivity, l is the distance between the two electrodes, and $a(t)$ is the plasma outer radius.

C. Detailed structure of the present work

As mentioned above, the main aim of the present research is to find a straightforward way to use one of the simple and very convenient models presented in Ref. 15 to obtain an acceptable estimate of the main characteristics of an underwater discharge. Based on Ref. 15, a two-phase model is proposed, termed *model A* and presented in the Appendix. *Model A* requires as input data the instantaneous power $\mathcal{P}_{PL}(t)$ related to the plasma resistance, something that cannot be obtained directly from the experimental data. A straightforward way to overcome this inconvenience would be calculating this power as a fraction k of the experimentally obtained total resistive power absorbed by the underwater discharge,

$$\mathcal{P}_{PL}(t) = k \cdot V_R \cdot I, \quad (5)$$

where $V_R = R_L \cdot I$ is the resistive part of the load voltage V_L. To demonstrate that this is possible, the following steps are followed:

(i)   Accurate experimental voltage and current data are obtained, from which the overall instantaneous absorbed power $V_R \cdot I$ is calculated.

(ii) Following the work presented in Ref. 21 a *simplified* 1D model, termed *model B*, is implemented using MATHCAD software.[30] The only difference from Ref. 21 is the use of an improved model for plasma conductivity, as suggested in Ref. 31. It is important to note that *model B* is capable of closely reproducing all results obtained with the most complete 1D model published in the literature.[20]

(iii) Using *model B* together with accurate pressure and bubble dynamics data, it is demonstrated that the input data required for *model A* to satisfactorily reproduce all the available experimental data require $k \approx 0.3$. In other words, the optimum input data for

model A represent 30% of the experimentally determined overall absorbed power.

(iv) Using as an optimum input Eq. (5) with $k = 0.3$, *model A* predictions are successfully tested against experimental data available in the literature.

The work to accomplish these steps is presented below.

III. PRACTICAL ARRANGEMENT

A. Power source and discharge electrodes

The equivalent electric scheme of the power source and its corresponding discharge electrodes is presented in Fig. 1. The power source is based on a capacitor bank having a capacitance $C_1 = 1.2$ mF charged to $V_0 = 1.5$ kV and storing 1350 J of electrostatic energy. For convenience, a simple but robust and reliable mechanical closing switch S is used to couple the transmission line (of self-inductance L_t in Fig. 1) and the load, i.e., the underwater discharge electrodes. During preliminary tests, *without the load being attached*, the overall equivalent resistance and self-inductance of the driving circuit have been determined as $R_b = 40$ mΩ and $L_1 = L_b + L_t = 4.3$ μH, where the self-inductance of the transmission line is $L_t = 3.2$ μH.

A horseshoe-shaped dielectric mount (Fig. 2) allows the high-power connections together with the two electrodes to be positioned accurately underwater. The electrodes are made from pure copper tubes,[32] with an outer diameter of 3 mm and an inner diameter of 1.2 mm and separated by a 7 mm gap. The gap was chosen during preliminary experiments, as an inter-electrode distance providing consistently reproducible results. Heat shrink tubing is placed onto electrodes to control the electric contact region and to stop spreading the plasma-metal contact, i.e., the electric contact is thus restricted to the cross section areas of the electrodes, as considered in all theoretical analysis. A 50 μm "pilot" wire made of pure copper[33] is used to initiate the discharge, with preliminary testing demonstrating that the quality of the electric contact with electrodes is not affecting the plasma discharge characteristics. This point is particularly important for the development of a future repetitive system.
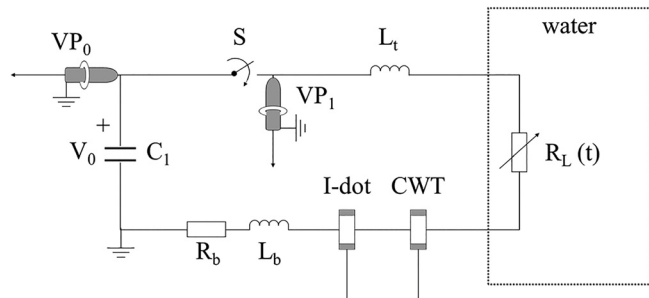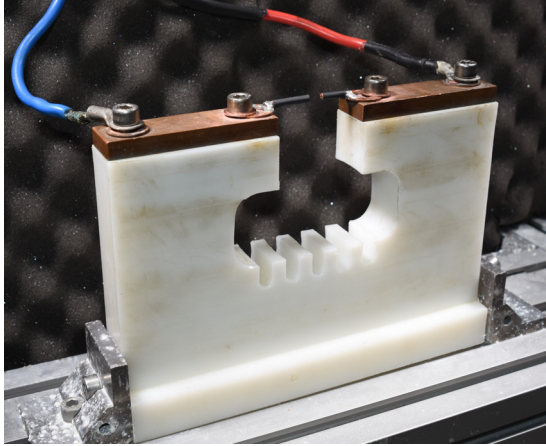

FIG. 1. Equivalent electric scheme of the system.

FIG. 2. (Color online) Horseshoe-shaped mount with high power connections and electrodes.

B. Water tank and semi anechoic enclosure

(i) *Water tank*. A 1100-litre glass-reinforced plastic (GRP) water tank with internal dimensions of $1190 \times 810 \times 1620 \, mm^3$[34] is filled with tap water and operated at a temperature between 22 °C and 24 °C. For accurate positioning, all the components of the underwater experimental arrangement are attached to a metallic frame (Fig. 3).

(ii) *Semi anechoic enclosure*. Eight acoustic AprFlex F28P absorbers $(200 \times 250 \times 10 \, mm^3)$,[35] with an absorbing frequency range between 1 and 20 MHz and with an echo-reduction varying from more than 20 dB at 1 MHz to larger than 40 dB above 6 MHz, are attached to a polyethene frame and positioned underwater forming an enclosure with the three hydrophones mounted at the center (Fig. 4).

C. Diagnostics

1. Electrical

(i) *Voltage in the main circuit*. Two voltage probes were used in the main circuit (VP in Fig. 1). VP_0 is a type PVM-5 probe[36] used for DC measurement during
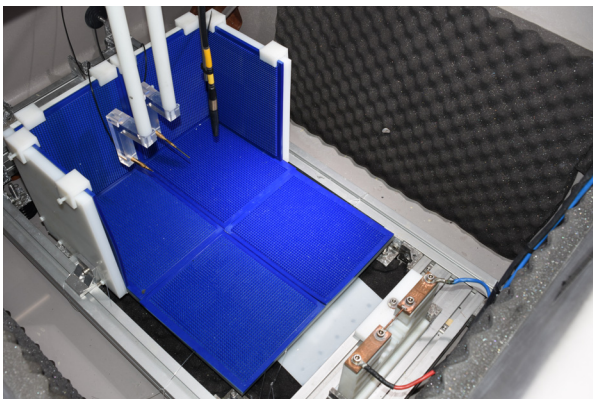

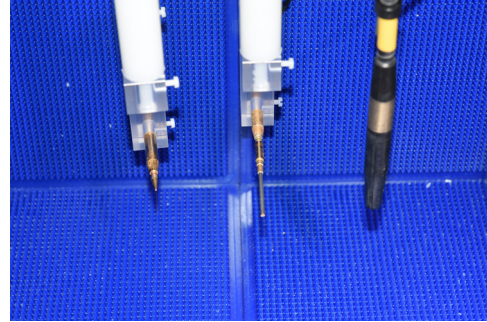FIG. 3. (Color online) Water tank assembly including the metallic frame.

FIG. 4. (Color online) The three hydrophones mounted in the semi anechoic enclosure. From left to right: NH0040, NH2000, and TC4034.

charging while VP_1, used to measure the voltage across the transmission line, is a type PVM-12 probe[36] capable of measuring a peak voltage impulse of 30 kV with a 90 MHz bandwidth.

(ii) *Current*. A current waveform transformer type 150B[37] (CWT in Fig. 1) can measure a peak current impulse of 30 kA with a bandwidth of 16 MHz.

(iii) *dI/dt*. An in-house developed Rogowski coil is used, which can be calibrated for each shot using the data obtained from the current sensor.

(iv) *Voltage across the underwater load*. This measurement is of paramount importance for obtaining accurate input data for the numerical model and therefore two very different methods of measuring this voltage have been used and compared during preliminary tests, as described below. For convenience, as both techniques provided the same results, only *method 1* is currently in use. It is encouraging that the two methods provide very close results, as *method 1* is based on *electric potential* measurement while *method 2* is based on *magnetic induction* measurement.

Method 1: In Fig. 5(a) voltage probe type PVM-5 is connected to the underwater electrodes (the load) through an insulated, short transmission line, having a very low self-inductance L_v. The probe itself, together with its ground connection, forms a loop having the self-inductance L_{vp} magnetically coupled with the transmission line through a mutual inductance M. By applying Kirchhoff's second law, the load voltage V_L can be obtained from the voltage measured by the voltage probe VP_L (on the order of 300 V) as

$$V_L(t) = VP_L(t) + V_{ind}(t), \qquad (6)$$

with the small inductive correction V_{ind} given by

$$V_{ind}(t) = (L_v + L_{vp} - 2M)\frac{dI_v}{dt} \qquad (7)$$

and where dI_v/dt is the very small value time rate-of-change of the current flowing through the transmission line. The inductive correction (on the order of -30 V) is obtained by performing tests with short-circuited electrodes. In this case $V_L \approx 0$ and the voltage probe directly measure the inductive correction, i.e., $VP_L \approx -V_{ind}$.
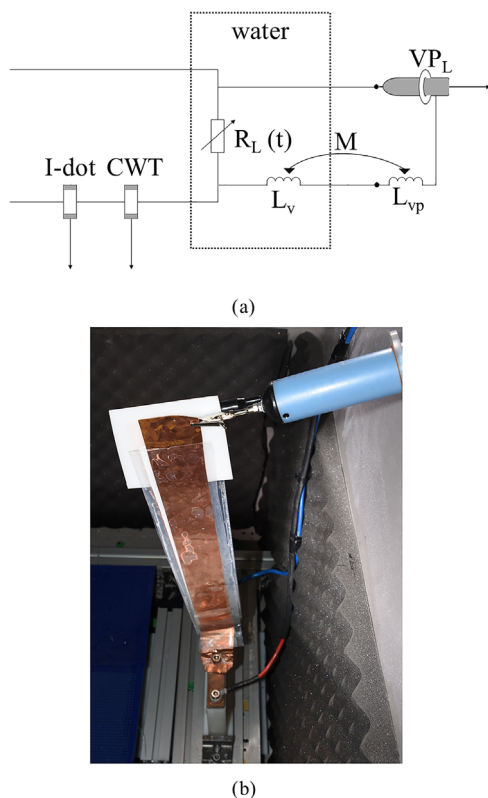
FIG. 5. (Color online) *Method 1* arrangement (a) equivalent electrical scheme, (b) real assembly.

The load voltage can be, in turn, written as

$$V_L(t) = R_L I + L_{PL} \frac{dI}{dt} + \frac{dL_{PL}}{dt} I, \qquad (8)$$

where L_{PL} is the time varying self-inductance of the plasma discharge and dL_{PL}/dt is the time rate-of-change of the plasma self-inductance.

Based on the results obtained with *model B*, the last two terms in the right-hand side of Eq. (8) can be neglected: for a 7 mm long plasma channel the L_{PL} is always smaller than 2 nH and the plasma dynamics indicates dL_{PL}/dt is on the order of -2.5×10^5 H/s, making $L_{PL}(dI/dt) + (dL_{PL}/dt)I < 0.2$ V. Therefore, in the present experiments, the approximation $V_R \approx V_L$ holds.

Important note: The voltage across the underwater load V_L can in principle be measured using the VP_1 of Fig. 1. In this case the voltage measured is $VP_1(t) = L_t(dI/dt) + V_L(t)$.

This is the method used in most published works, for example, in Refs. 20, 22, 27, and 28. However, the first term (the inductive voltage correction) is usually much larger than the second term. Preliminary tests performed with VP_1 demonstrated the load voltage measurement using this technique is not accurate. The main reason is related to the large value of the discharge current time rate-of-change dI/dt. Hence the reason *method 1* described above has been implemented: in such a case, the time rate-of-change of the current flowing through the voltage probe dI_v/dt is many orders of magnitude smaller than dI/dt.

Method 2: The schematic of this arrangement is presented in Fig. 6, where a non-inductive resistor[38] $R_v = 27\ \Omega$ is mounted in parallel to the underwater load and the current through this resistor I_{CT} is measured using a current transformer CT,[39] capable of measuring a peak current impulse of 500 A with a bandwidth of 35 MHz. The assembly is mounted inside an acrylic tube (see Fig. 6) and positioned underwater. In this case the load voltage V_L is directly obtained as

$$V_L(t) = R_V I_{CT}. \qquad (9)$$

2. Acoustical

(i)   *Low frequency hydrophone*. Teledyne Reson type TC4034,[40] having a usable frequency range from 1 Hz to 480 kHz. This hydrophone is omnidirectional across its bandwidth. The calibration data are provided by the manufacturer as a variable response over the whole bandwidth.

(ii) *High frequency hydrophones*. Two Precision Acoustics needle type of hydrophones were used. The first is a 2 mm needle PVDF hydrophone type NH2000,[35] suitable for measurements in the frequency range from 100 kHz to 10 MHz. The NH2000 is highly directional, particularly for high frequencies, and so great care was taken during its alignment. The second hydrophone is a 40 μm needle PVDF hydrophone type NH0040,[35] suitable for measurements in the frequency range from 1 to 40 MHz. When compared with NH20000, the NH0040 is less directional. For both needle-type hydrophones, the
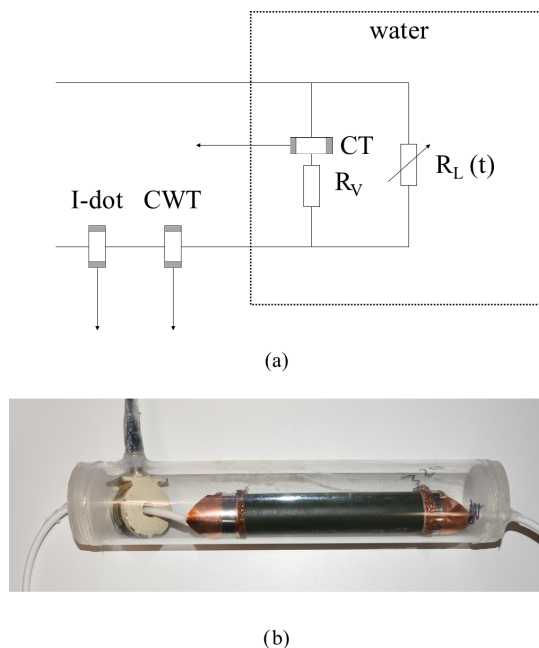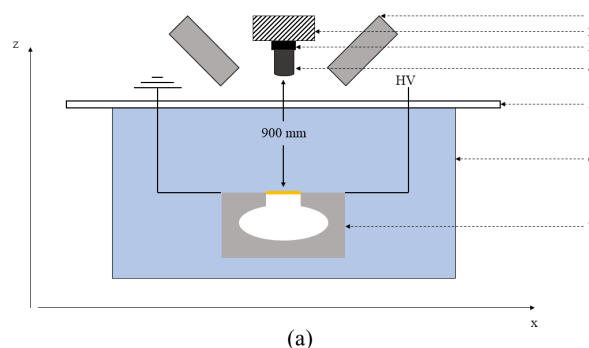

FIG. 6. (Color online) *Method 2* arrangement (a) equivalent electrical scheme, (b) assembly mounted inside an acrylic tube positioned underwater.

calibration data were obtained from the National Physics Laboratory (UK) as a variable response over their entire characteristic bandwidths.
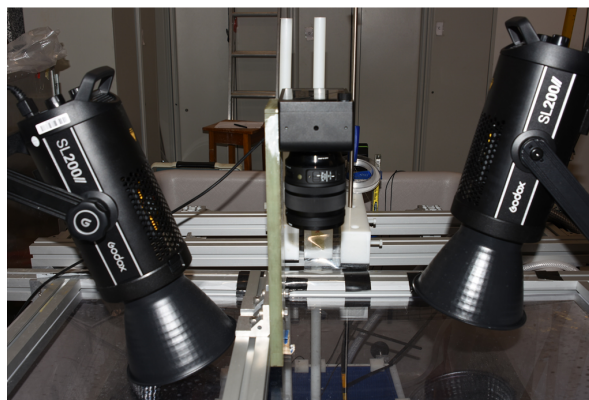
(iii)   *Details of hydrophone mounting and operation.* Apart from a very expensive fibre-optic based hydrophone used in Ref. 28, there is no hydrophone to cover the whole frequency bandwidth required by the phenomena: from Hz to tens of MHz. Therefore, the three different hydrophones presented above are all mounted using supports as shown in Fig. 4 and placed at the minimum separation from one another that allowed for the full pressure wave to be captured by each hydrophone before any reflection from the other would be detected and influence the signal. All hydrophones displayed sensitivity to the powerful electromagnetic noise generated by the operation of the pulsed power generator but, when mounted at least 0.5 m away from the source they were capable of fully recovering, well before the pressure waves were recorded.

(iv)   *Software and data analysis.* A MATHCAD[30] program was developed to analyze the data obtained from the three hydrophones. To help with the alignment of the highly directional NH2000 hydrophone, the software was used to test agreement with the TC4034 signal in the overlapping receiving bandwidth (i.e., from 100 to 480 kHz). As already mentioned, no hydrophone is individually capable to cover the ultrawide spectrum generated by the source, and therefore the software is used to perform the FFT of each of the pressure signals, calibrate the FFT using the corresponding frequency response data and then trim and stitch the three signals in the frequency domain, before performing the inverse FFT to obtain the pressure signal in the time domain corresponding to the entire bandwidth covered (i.e., from 1 Hz to 40 MHz).

3. Optical

A Chronos 2.1-HD high-speed camera[41] operating at 6000 frames per second (fps) with a 133.5 μs exposure for obtaining good resolution photos (640×360 pixels) is positioned directly above the discharge (see Fig. 7). For detecting details of the bubble dynamics however, the camera is also operated at 20 000 fps with a 3.9 μs exposure and at a lower resolution (640×96 pixels). A FotodioX Nikon F to C-Mount lens adapter is used to attach a Sigma 24–70 mm f/2.8 zoom lens to the camera. As the plasma is emitting a very bright light at the start of the discharge, a Hoya PROND8 Neutral Density (ND) filter is required to be supplementary attached to the Sigma lens to protect the camera from overexposure. Two Godox Sl-200W II LED lights (see Fig. 7) are positioned to provide the necessary lighting to detect the bubble dynamics during its late expansion stages. To protect the camera and the LED lights from shock wave generated damage, a polycarbonate sheet

(a)

(b)

FIG. 7. (Color online) (a) Schematic of the arrangement of electrodes, high-speed camera and lighting (not to scale). (1) Godox SL-200W II LED light, (2) Chronos 2.1-HD high-speed camera, (3) FotodioX Nikon F to C-Mount lens adaptor, (4) Sigma 24-70 mm f/2.8 zoom lens, (5) polycarbonate sheet, (6) water tank, (7) horseshoe-shaped mount (b) the real arrangement.

($1000 \times 500 \times 10 \, \text{mm}^3$) is placed above the tank between the instruments and the water.

IV. EXPERIMENTAL RESULTS AND COMPARISON WITH THEORETICAL PREDICTIONS

A. Experimental data

The experiments provided data with a high level of reproducibility. The complete set of data obtained from a single shot is provided in Figs. 8–11.

The use of the pilot wire generates a two-step process: first, the exploding wire (EW) creates a plasma column that in turn triggers the underwater discharge.

A sophisticated code, like the one presented in Ref. 42 is required to obtain all the details of an underwater EW phenomenon, but that is unnecessary for the present work. A 2D underwater EW model is an extremely complex numerical model and not required as the EW is only used to reproducibly generate the plasma column and is not necessary for understanding the discharge phenomena. Using an existing simple phenomenological model for the underwater EW resistivity,[43] the current through and the voltage across the pilot wire during explosion are both calculated and successfully compared in Figs. 8 and 10 (see the insets) with experimental data. Towards the end of the EW process, the wire resistance increases by two orders of magnitude, literally
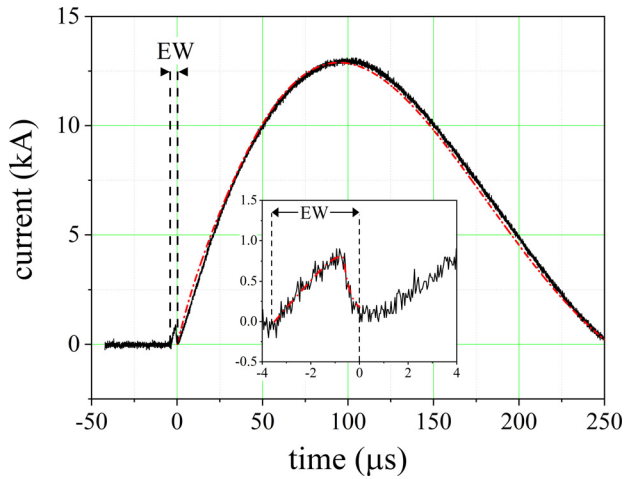
FIG. 8. (Color online) Discharge current measured with CWT of Fig. 1 (*full line*) is compared with an EW model (see inset) and with predictions made by *model B*. The theoretical predictions (*dash-dotted lines*) are practically indistinguishable. To facilitate the comparison, the time origin is chosen at the time the plasma discharge begins, *after* the "pilot" wire exploded. The inset presents details of the current during the EW action.
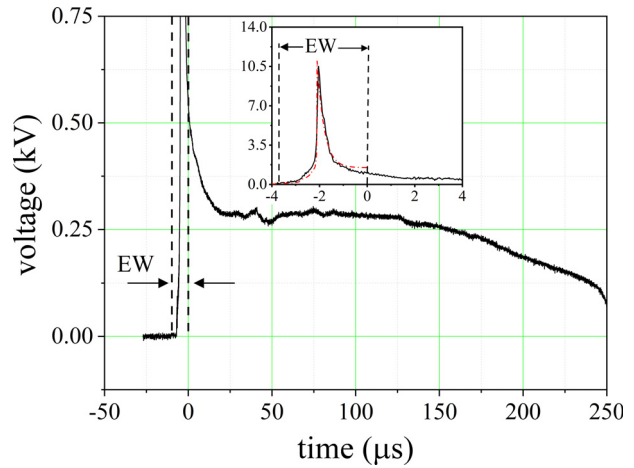

FIG. 10. (Color online) Voltage across the load obtained using *method 1* of Fig. 5. The time origin as in Fig. 8. The inset shows the large voltage (10.5 kV) generated during the EW action (*full line*), compared with an EW model (*dash-dotted line*).

acting like an "opening switch," i.e., the current (Fig. 8, inset) returns to (almost) zero. Once the EW-generated plasma channel resistance starts to lower its value, the circuit "closes" again and the plasma discharge begins as a second step of the process. It is important to note that the energy consumed by the EW phenomenon is extremely small, i.e., only 2.4 J, representing less than 0. 2% of the initially stored energy. However, during the very short time the wire explodes, intense shock waves are generated, and the hydrophones detect the corresponding pressure impulse (Figs. 11 and 12).

It is interesting to note that during the EW action the efficiency of energy conversion, from the total electromagnetic (Joule) energy absorbed to acoustic (mechanic) energy generated is estimated to be more than 10%, as presented elsewhere.[44] This is a high efficiency when compared with
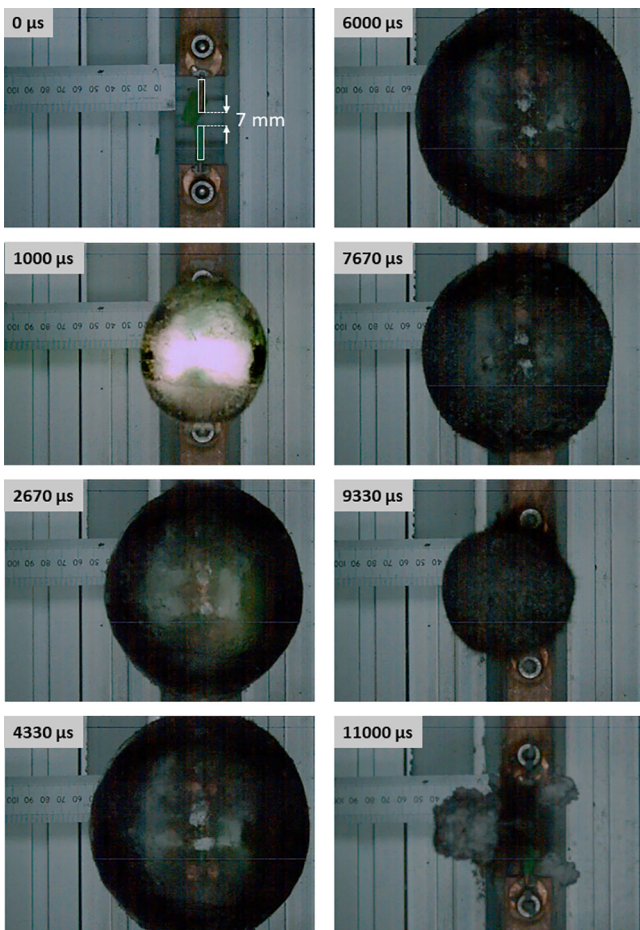

FIG. 9. (Color online) Photos taken with the high-speed camera operated at 6000 fps showing the bubble dynamics. Time origin from switch S (Fig. 1) action.
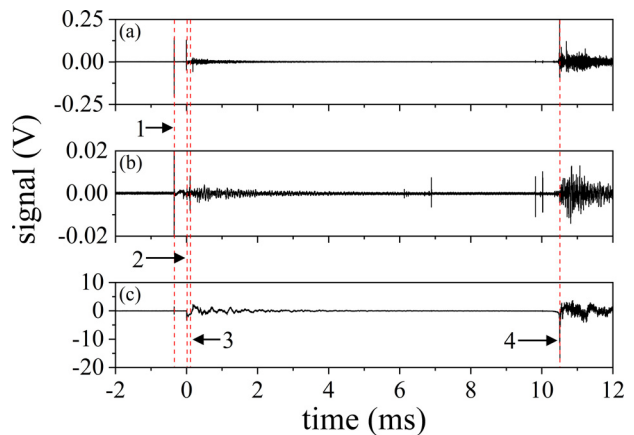

FIG. 11. (Color online) Oscilloscope raw data obtained from the three hydrophones. *Vertical dashed lines*: 1—large initial electromagnetic interference at the time the switch S in Fig. 1 closes. 2—EW phenomenon. 3—underwater discharge and 4—pressure generated by bubble implosion (a) positive signal from the 2 mm needle hydrophone, (b) negative signal from 40 μm needle hydrophone, (c) negative signal generated by the Reson hydrophone.
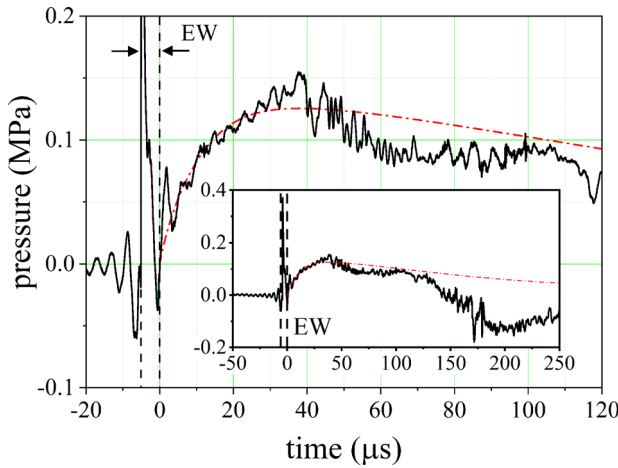
2850   J. Acoust. Soc. Am. **151** (5), May 2022

Frost *et al.*

FIG. 12. (Color online) Experimental (relative) pressure impulse at $r = 0.5\,\mathrm{m}$ distance from the source (full line), compared with predictions obtained using *model A* (*dashed-dotted line*). Time origin as in Fig. 8.

only 1.8% for the plasma discharge that follows. The last figure is also in good agreement with published data.[12]

B. Obtaining the optimum input data for model A

As described in the plan detailed above, *model B* is only used in this work to facilitate obtaining a value for the fraction k in Eq. (5). As expected, the current predicted by *model B* is perfectly matching the experimental data of Fig. 8 and the calculated power absorbed by the plasma $\mathscr{P}_{PL}(t)$ is presented in Fig. 13, where the overall power absorbed by the load, obtained from the data in Figs. 8 and 10 as $V_R \cdot I$, is also shown. As demonstrated in Fig. 13, the theoretical prediction favorably compares with 30% of the overall experimental power, i.e., $k = 0.3$. As one may expect by simplifying k to a time constant, the match is not perfect but, as further shown below, this straightforward technique to generate input data is good enough to allow *model A* to generate credible predictions.
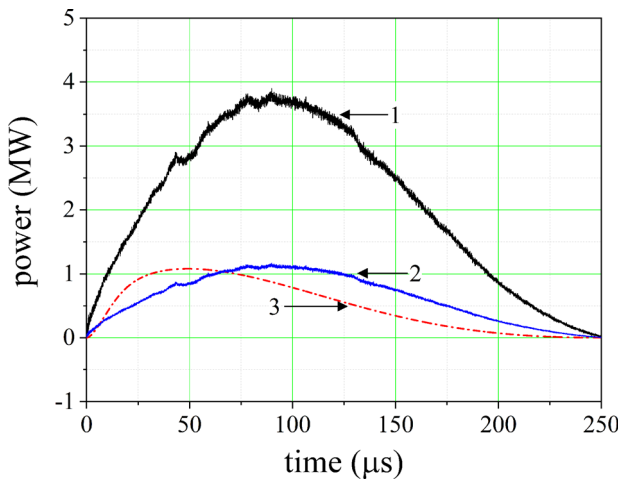

FIG. 13. (Color online) *Line 1 (full)*: overall power $V_R I$ absorbed by load. *Line 2 (full)*: the fraction $k\, V_R I$ of the overall power, for $k = 0.3$ [see Eq. (5)] used as input data $\mathscr{P}_{PL}(t)$ for the *model A* presented in the Appendix. *Line 3 (dashed-dotted)*: theoretical prediction using *model B* for the power absorbed by the plasma. Time origin as in Fig. 8.
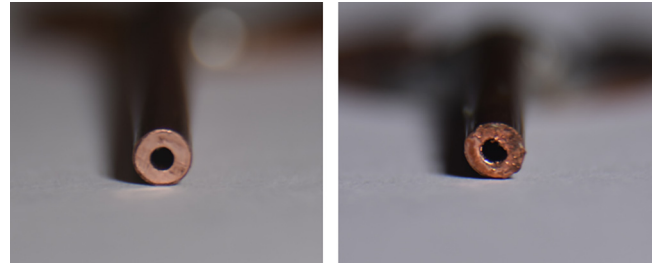

FIG. 14. (Color online) Underwater electrode. *Left*: pristine condition; *Right*: after one shot.

C. Model A predictions

Model A, using the input data shown in Fig. 13, can now be used to predict the main measurable characteristics of the underwater discharge. *Model A*, detailed in the Appendix, is structured as a two-phase model, with each phase needing the integration of first-order differential equations. The integration time is referred from $t_0 = 0\ \mu\mathrm{s}$ to $t_1 = 250\ \mu\mathrm{s}$ for the first fast phase, which mainly deals with predictions of pressure generation. The integration of the second slower phase, between $t_1 = 250\ \mu\mathrm{s}$ and $t_2 = 11.2\,\mathrm{ms}$, provides a prediction of the bubble dynamics. The results, presented in Figs. 14 and 15, require the comments below.

In Fig. 12, the pressure impulse predicted by *model A* is initially very close to experimental data. However, after about $125\ \mu\mathrm{s}$, the experimental pressure drops faster than predicted, a phenomenon that can be observed in other works as well.[20] This may be related to the development of other types of energy loss phenomena, with their corresponding resistance term being R_O in Eq. (2). One possible candidate is electrode erosion. Indeed, photos taken after only one shot (see Fig. 14), clearly show the electrode surface in contact with plasma being affected. These phenomena require further investigation.

In Fig. 15 the bubble oscillating period is accurately predicted by *model A*. The dynamics of the experimental
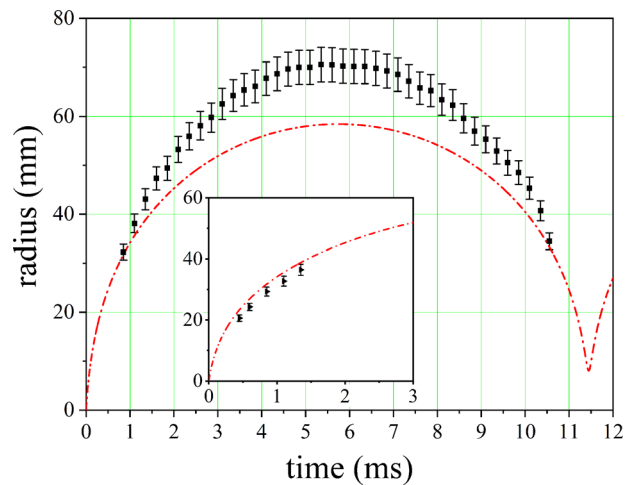

FIG. 15. (Color online) Dynamics of the plasma bubble. The time variation of the outer radius $a(t)$, as predicted by *model A*, is compared with data points obtained using the high-speed camera. The inset shows that a much better comparison is obtained if the experimental points are considered to follow the "lighted" region of the bubble. Time origin as in Fig. 8.

J. Acoust. Soc. Am. **151** (5), May 2022

Frost *et al.* 2851

outer radius of the bubble, detected as a black spherical cloud, is somewhat different from the theoretical estimation. In the inset of Fig. 15, however, where early experimental data detected as a luminous sphere are shown, the match between theory and experiment is extremely close.

Unfortunately, the luminous sphere is covered by the black cloud at later times. As the plasma is heated at temperatures on the order of a few tens of thousands of degrees, the black cloud may not represent faithfully the plasma outer boundary.

In conclusion, *model A* can produce a reasonable estimate of the experimentally determined characteristics of the present underwater discharge.

D. Model A predictions for data available in the literature

As the last step in validating the suggested technique, it is essential to consider, for a wide range of practical underwater discharge arrangements, how close to experimental data are the *model A* predictions. Table I presents the main characteristics of several underwater discharge systems presented in the literature, for which pressure and/or bubble dynamics data are provided, together with electrical data required to calculate the input for *model A*. The criterion for a pressure pulse to be compared with theoretical predictions is to be measured far from the region where shock waves are present, in which case Eq. (A5) in the Appendix is applicable. In all cases, *model A* uses as input Eq. (3) with $k = 0.3$, with the power calculated from the published experimental current and voltage data.

(i)   In Fig. 16, the experimental pressure pulse and the corresponding bubble dynamics published in Refs. 12 and 25 are successfully compared with predictions made using *Model A*.

(ii) In Fig. 17, the variation of the peak pressure pulse with the peak current impulse as well as a typical experimental pressure pulse published in Ref. 14 are both successfully compared with predictions made using *model A*.

(iii) In Fig. 18, the bubble dynamics data published in Ref. 20 is compared with predictions made using *model A*. Interestingly, the prediction made by *model A* is in this case better than that made by the best 1D code published in the open literature.[20]
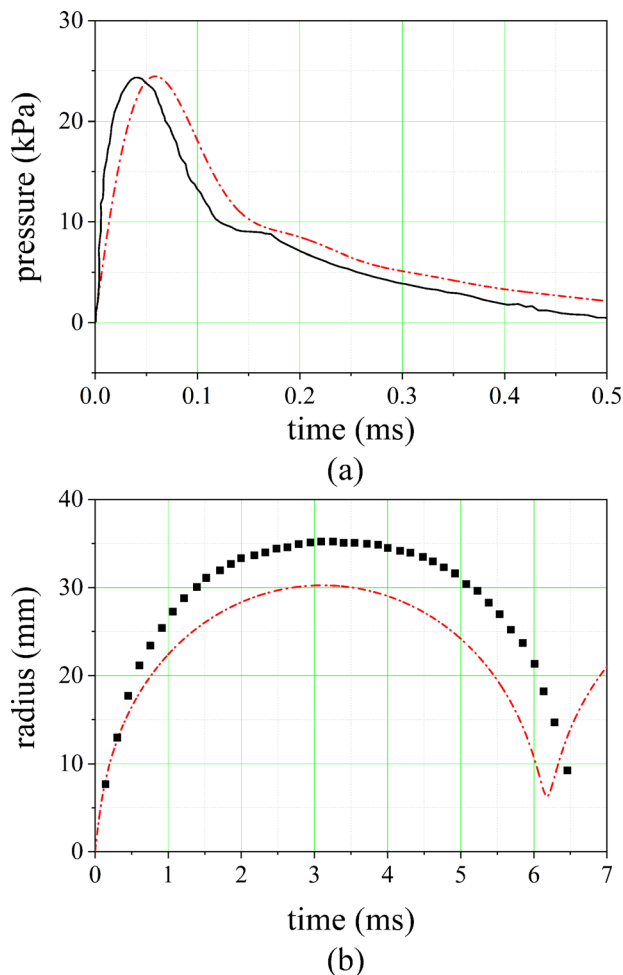

FIG. 16. (Color online) Comparison between experimental data taken from Refs. 12 and 25 and predictions made using *model A* with input obtained from experimental electric data. (a) Pressure impulse: experimental data (*continuous line*) and *model A* predictions (*dot-dashed line*). (b) Bubble dynamics: experimental data (*full squares*) and *model A* predictions (*dot-dashed line*).

(iv) In Fig. 19, the experimental pressure pulse presented in Ref. 22 is successfully compared with the prediction made using *model A*.

Overall, as demonstrated, *model A* can adequately estimate the main measurable characteristics produced by various underwater discharge systems.

E. Suggested methodology for using model A for designing and optimizing a new system for generating acoustic pressure pulses

During preliminary discharges, with the load short circuited and with reference to Fig. 1, the main circuit parameters of the power supply are obtained as C_1, V_0, L_b, L_t, and R_b. A subsequent stage of development is recommended, in which the load (i.e., the electrode assembly) is placed inside a small water bucket, with the load voltage and current accurately measured as described above (e.g., *method 1*). The measured resistive power $V_R \cdot I$ is then introduced in Eq. (3) and, with $k = 0.3$, these data are used as

TABLE I. Main characteristics of underwater discharge systems.

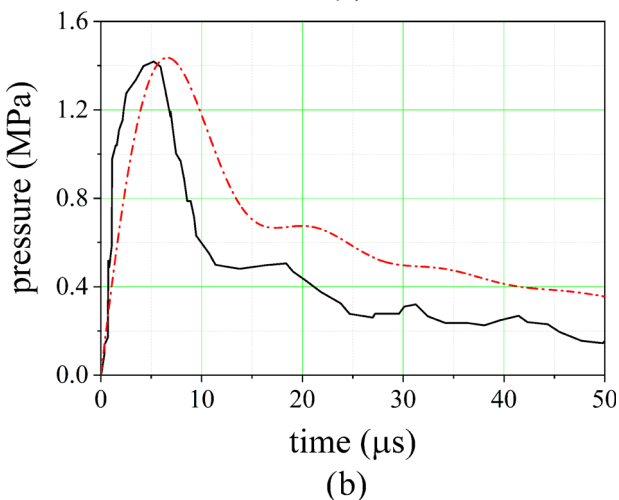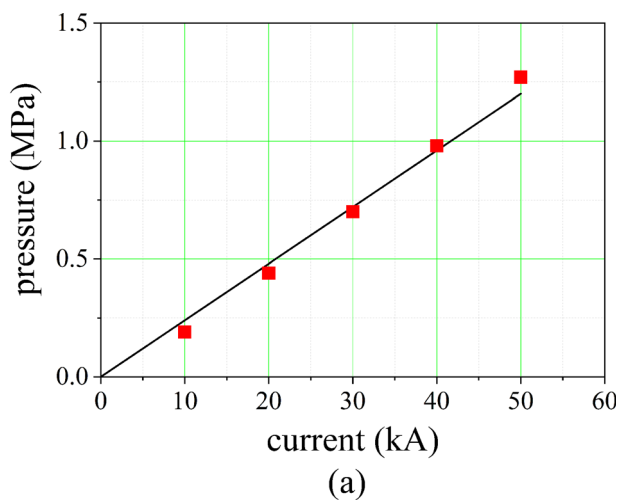| Reference	Energy stored in the capacitor bank (kJ)	Period of discharge (μs)	Fig. number
12, 25	0.625	245	16
14	from 0.27 to 6.6	25.4	17
20	0.51	30	18
22	0.21	25	19
Present work	1.35	451	13 and 15

FIG. 17. (Color online) Comparison between experimental data taken from Ref. 14 and predictions made using *model A* with input obtained from experimental electric data. (a) Peak pressure variation with peak current: experimental data (*straight line*) from Ref. 14 and *model A* predictions (*full squares*). (b) typical pressure pulse: experimental recorded data (*continuous line*) from and *model A* predictions (*dot-dashed line*).

FIG. 19. (Color online) Comparison between experimental data taken from Ref. 22 (*continuous line*) and *model A* predictions (*dot-dashed line*). On the timescale presented in Ref. 22, the two are indistinguishable.

input for *model A*. The code in turn provides an estimate of the acoustic pressure pulse that can be generated in water at various distances from the source. During the early developmental stages of a new system, these simple tests, together with *model A*, will help avoid the need for both a large water tank and the use of complex and expensive diagnostic equipment.

V. CONCLUSIONS AND THE WAY AHEAD

The present work demonstrates the following:

(i)   The plasma resistance of an underwater discharge phenomenon cannot be directly measured; it can only be calculated using a 1D model.

(ii)   Accurately measuring the voltage generated across a pair of underwater discharge electrodes requires a dedicated arrangement.

(iii) Using 30% of the overall instantaneous resistive power absorbed by an underwater discharge as an input for a simple two-phase numerical code, can provide a straightforward and satisfactory solution to estimate the main discharge characteristics.

The work also highlights several important practical details to be observed during underwater discharge experiments.

There is an increased worldwide interest in using underwater discharges to generate pressure impulses for modern applications such as those related to the food industry and e-waste disposal. In most cases, the research teams will not have the time to develop a complex 1D model for predicting the characteristics of the underwater discharge and guide the design of an optimized arrangement. In such situations, the simple theoretical techniques and the methodology presented in this work will be of great use for a wide range of systems operated with initial energy between 0.2 and 6.6 kJ and having a characteristic discharge period between 25 and 450 μs.
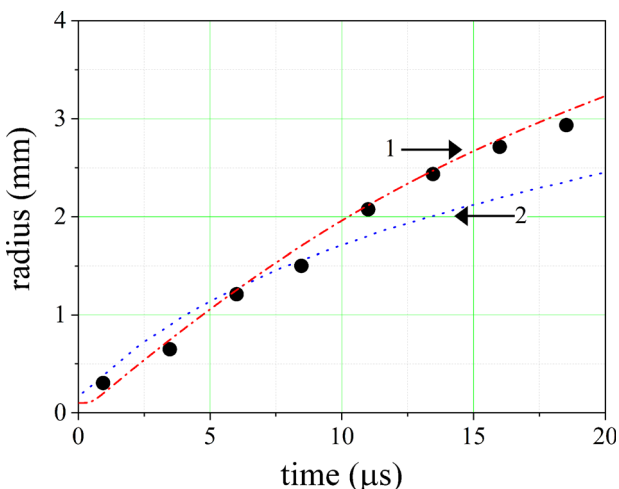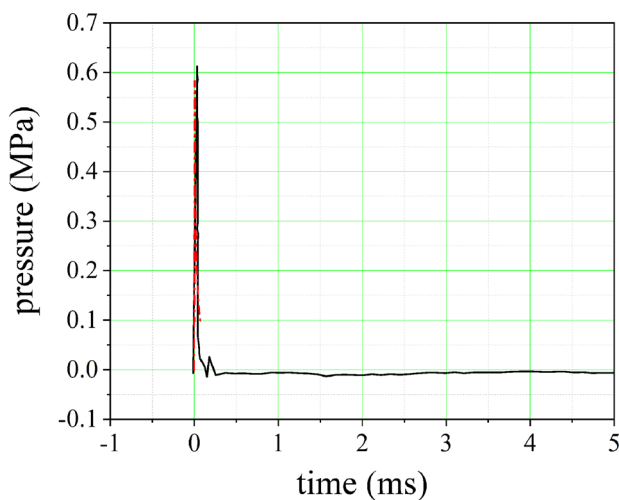

FIG. 18. (Color online) Comparison between experimental data (*full circles*) taken from Ref. 20 and theoretical predictions made by: *Line 1* (*dashed-dotted*): *model A*, *Line 2* (*dotted*): 1D code (Ref. 20).

The way ahead will be dedicated to the development of a low repetition rate system for generating acoustic pressure pulses. The work will include implementing a semiconductor-based closing switch in the present power circuit and manufacturing a mechanism for feeding the exploding wire used to trigger the discharge.

APPENDIX

Model A is constructed in two parts, both based on the work presented in Ref. 15 and considers the water as a compressible medium. The equations of this simple model are presented below in their most compact form, ready to be implemented in any mathematical software. For a comprehensive description, however, Ref. 15 must be consulted.

In what follows:

Variables to be integrated:

- $a(t)$ is the radius of the plasma bubble
- $v(t)$ is the expansion velocity of the plasma bubble
- $p(t)$ is the pressure inside the plasma bubble

Various constants:

- $p_0 = 10^5$ Pa is the (initial) atmospheric pressure
- $\gamma = 1.3$ is a constant representing the ratio of specific heats
- $A = 3001 \times 10^5$ Pa, $B = 3000 \cdot 10^5 \times$ Pa and $n = 7$ are all constants used in Tait's equation of state of water
- $\rho_0 = 10^3$ kg/m^3 is the density of water at $p = p_0$
- $c_0 = 1450$ m/s is the speed of sound in water at $p = p_0$

Various functions:

- $c(t)$ is the speed of sound in compressed water:

$$c(t) = \sqrt{\frac{nA^{1/n}}{\rho_0}(p(t)+B)^{(n-1)/n}}. \tag{A1}$$

It is easy to demonstrate that at $t = 0$, when $p(0) = p_0$ then $c(0) = c_0$.

- $h(t)$ is the specific enthalpy and dh/dt its time rate-of-change,

$$h(t) = \frac{c_0}{n-1}\left[\left(\frac{p(t)+B}{A}\right)^{(n-1)/n} - 1\right], \tag{A2}$$

$$\frac{dh}{dt} = \frac{c_0}{nA}\left(\frac{A}{p(t)+B}\right)^{1/n}F(t), \tag{A3}$$

where the function $F(t)$ is

$$F(t) = \frac{3(\gamma-1)}{4\pi a(t)^3}\left(\mathcal{P}_{PL}(t) - \frac{\gamma}{\gamma-1}4\pi a(t)^2 p(t)v(t)\right) \tag{A4}$$

and where $\mathcal{P}_{PL}(t) = k \cdot V_R \cdot I$ represents input data, i.e., the power absorbed by the plasma (see the text).

The integration is performed in two phases, as described below.

Phase 1: in which the plasma absorbs energy, and the flow is compressible. This phase begins at $t = 0$ and ends at a time $t = t_1$, when the power absorbed returns to zero.

Phase 2: in which the bubble is expanding adiabatically. This phase begins at $t = t_1$ and can be extended to any chosen time $t = t_2$, to allow comparison with the bubble dynamics data recorded by a video camera.

1. Phase 1

The *first-order differential system of equations* to be integrated from $t = 0$ to $t = t_1$ is

$$\frac{dv}{dt} = \frac{\left(1+\frac{v(t)}{c(t)}\right)h(t) + \frac{a(t)}{c(t)}\left(1-\frac{a(t)}{c(t)}\right)\frac{dh}{dt} - \frac{3}{2}v(t)^2\left(1-\frac{v(t)}{c(t)}\right)}{a(t)\left(1-\frac{v(t)}{c(t)}\right)},$$

$$\frac{da}{dt} = v(t),$$

$$\frac{dp}{dt} = F(t),$$

with the *initial conditions*

$v(0) = 0.01$ m/s,
$a(0) = 0.1 \times 10^{-3}$ m,
$p(0) = p_0$.

As noticed in Ref. 15, the results are not very sensitive to the chosen initial conditions. The final integrated values are $v(t_1)$, $a(t_1)$ and $p(t_1)$.

2. Phase 2

The *first-order differential system of equations* to be integrated from $t = t_1$ to $t = t_2$ is

$$\frac{dv}{dt} = \frac{1}{a(t)}\left[\frac{p(t_1)}{\rho_0}\left(\frac{a(t_1)}{a(t)}\right)^{3\gamma} - \frac{3}{2}v(t)^2 - \frac{p_0}{\rho_0}\right],$$

$$\frac{da}{dt} = v(t),$$

with the *initial conditions* $v(t_1)$ and $a(t_1)$ obtained from *Phase 1*.

After the integration is performed, and to allow a comparison with pressure data obtained from hydrophones, the pressure P generated at a distance r from the discharge is estimated as

$$P(r,\bar{t}) = A\left\{\frac{2}{n+1} + \frac{n-1}{n+1}\left[1 + \frac{n+1}{rc_0}G(\bar{t})\right]^{1/2}\right\}^{(2n/n-1)} - B - p_0, \tag{A5}$$

where the time dependent function $G(t)$ is

$$G(t) = a(t)\left[h(t) + \frac{v(t)^2}{2}\right]. \tag{A6}$$

Equation (A5) *is only valid for acoustic pressures and therefore the distance r must be large enough to damp the influence of the shock waves.*

Note that to make it easier to compare the pressure calculated with Eq. (A5) with the hydrophone data:

- A "retarded" time $\bar{t} = t - r/c_0$ is considered.
- The pressure is calculated relative to p_o, i.e., the initial pressure calculated with Eq. (A5) is zero.

[1]*Bmax*, https://www.bmax.com/technology/electro-hydraulic-forming/ (Last viewed 12/14/2021).

[2]J. Hofmann and T. H. Weise, "Pulsed power technologies for commercial material reduction and crushing applications," in *Proceedings of the 11th IEEE International Pulsed Power Conference*, Baltimore, MD (1997), pp. 203–207.

[3]K. J. Touryan, L. A. Touryan, and J. W. Benze, "An innovative use of pulsed power technology for separation of minerals from ores," in *Proceedings of the 8th IEEE International Pulsed Power Conference*, San Diego, CA (1991), pp. 90–93.

[4]G.-H. Rim, C.-H. Cho, H.-S. Lee, and E. P. Pavlov, "An electric-blast system for rock fragmentation," in *Proceedings of the 12th IEEE International Pulsed Power Conference*, Monterey, CA (1999), pp. 165–168.

[5]S. Pronko, G. Schofield, M. Hamelin, and F. Kitzinger, "Megajoule pulsed power experiments for plasma blasting mining applications," in *Proceedings of the 9th IEEE International Pulsed Power Conference*, Albuquerque, NM (1993), pp. 11–18.

[6]I. V. Lisitsyn, H. Inoue, S. Katsuki, H. Akiyama, and I. Nishizawa, "Drilling and demolition of rocks by pulsed power," in *Proceedings of the 12th IEEE International Pulsed Power Conference*, Monterey, CA (1999), pp. 169–172.

[7]S. Boev and N. Yavorovsky, "Electropulse water treatment," in *Proceedings of the 12th IEEE International Pulsed Power Conference*, Monterey, CA (1999), pp.181–184.

[8]M. Sato, T. Ohgiyama, and J. S. Clements, "Formation of chemical species and their effects on microorganisms using a pulsed high-voltage discharge in water," IEEE Trans. Ind. Appl. **32**(1), 106–112 (1996).

[9]M. S. Mazzola, M. G. Grothaus, M. Walch, and J. Jones-Meehan, "New electrical control methods to prevent power plant fouling," in *Proceedings of the 10th IEEE International Pulsed Power Conference*, Albuquerque, NM (1995), pp. 34–39.

[10]H. Akiyama, S. Sakai, T. Sakugawa, and T. Namihira, "Environmental applications of repetitive pulsed power," IEEE Trans. Dielectr. Electr. Ins **14**(4), 825–833 (2007).

[11]J. W. Mackersie, I. V. Timoshkin, and S. J. MacGregor, "Generation of high-power ultrasound by spark discharges in water," IEEE Trans. Plasma Sci. **33**(5), 1715–1724 (2005).

[12]S. Buogo and J. Plocek, "Efficiency of energy conversion in underwater spark discharges and associated bubble oscillations: Experimental results," Acta Acust. Acust. **95**, 46–59 (2009).

[13]V. Y. Ushakov, V. F. Klimkin, and S. M. Korobeynikov, *Impulse Breakdown of Liquids* (Springer, Berlin, 2007).

[14]Y. Bacqueyrisses, T. Reess, A. Silvestre de Ferron, V. Tchalla, and B. M. Novac, "Phenomenological studies for optimizing subsonic underwater discharges," IEEE Trans. Plasma Sci. **49**(11), 3615–3624 (2021).

[15]K. A. Naugol'nykh and N. A. Roi, "Spark discharges in water (a hydrodynamical description)," *NOAA Technical Memorandum OAR ETL-300*, December 2000, National Oceanic and Atmospheric Administration, Environmental Technology Laboratory Boulder, CO (Nauka, Moscow, 1971) (in Russian).

[16]J. W. Robinson, M. Ham, and A. N. Balaster, "Ultraviolet radiation from electrical discharges in water," J. Appl. Phys. **44**(1), 72–75 (1973).

[17]V. T. Gurovich, A. Grinenko, Y. E. Krasik, and J. Felsteiner, "Simplified model of underwater electrical discharge," Phys. Rev. E **69**, 036402 (2004).

[18]O. A. Sinkevich and A. L. Shevchenko, "Numerical investigation of electric discharge in water," Fluid Dyn. **18**(3), 422–426 (1983).

[19]X. Lua, "One-dimensional bubble model of pulsed discharge in water," J. Appl. Phys. **102**, 063302 (2007).

[20]K.-J. Chung, S.-G. Lee, Y. S. Hwang, and C. Y. Kim, "Modeling of pulsed spark discharge in water and its application to well cleaning," Curr. Appl. Phys. **15**(9), 977–986 (2015).

[21]A. W. H. Kratel, "Pulsed power discharges in water," Ph.D. dissertation, California Institute of Technology, Pasadena, CA (1996).

[22]X. Lu, Y. Pan, K. Liu, M. Liu, and H. Zhang, "Spark model of pulsed discharge in water," J. Appl. Phys. **91**(1), 24–31 (2002).

[23]J. W. Robinson, "Finite-difference simulation of an electrical discharge in water," J. Appl. Phys **44**, 76–81 (1973).

[24]A. I. Vovchenko, V. V. Kucherenko, and V. V. Shamko, "Characteristics of the space-time evolution of vapor-gas cavities generated by an underwater spark discharge," J. Appl. Mech. Tech. Phys. **19**(6), 755–760 (1978).

[25]S. Buogo and G. B. Cannelli, "Implosion of an underwater spark-generated bubble and acoustic energy evaluation using the Rayleigh model," J. Acoust. Soc. Am. **111**(6), 2594–2600 (2002).

[26]A. I. Ioffe, "Theory of the initial stage of an electrical discharge in water," J. Appl. Mech. Tech. Phys. **7**(6), 47–50 (1971).

[27]I. V. Timoshkin, R. A. Fouracre, M. J. Given, and S. J. MacGregor, "Hydrodynamic modelling of transient cavities in fluids generated by high voltage spark discharges," J. Phys. D: Appl. Phys. **39**, 4808–4817 (2006).

[28]V. Stelmashuk, P. Hoffer, K. Kolacek, and J. Straus, "Experimental study of spark channel expansion in water," IEEE Trans. Plasma Sci. **48**(2), 491–499 (2020).

[29]C. Balanis, *Antenna Theory: Analysis and Design*, 3rd ed. (Wiley-Blackwell, Hoboken, NJ, 2005).

[30]PTC Mathcad, https://www.mathcad.uk/ (Last viewed 12/14/2021).

[31]K. J. Chung and Y. S. Hwang, "Thermodynamic properties and electrical conductivity of water plasma," Contrib. Plasma Phys. **53**(4-5), 330–335 (2013).

[32]Goodfellow, https://www.goodfellow.com/uk/en-gb (Last viewed 12/14/2021).

[33]Advent, https://www.advent-rm.com/en-GB/ (Last viewed 12/14/2021).

[34]Kingfisher, https://www.kingfisherdirect.co.uk/ (Last viewed 12/14/2021).

[35]Precision Acoustics, https://www.acoustics.co.uk/ (Last viewed 12/14/2021).

[36]North Star, https://www.highvoltageprobes.com/products/high-voltage-probes/ (Last viewed 12/14/2021).

[37]Power Electronics Measurements, http://www.pemuk.com/products/cwt-current-probe/cwt.aspx (Last viewed 12/14/2021).

[38]HVR International, http://www.hvrint.com/ (Last viewed 12/14/2021).

[39]Stangenes Industries, Inc., https://www.stangenes.com/ (Last viewed 12/14/2021).

[40]Teledyne Marine, http://www.teledynemarine.com/reson-tc-4034/?BrandID=17 (Last viewed 12/14/2020).

[41]Kron Technologies, https://www.krontech.ca/ (Last viewed 12/14/2021).

[42]K.-J. Chung, K. Lee, Y. S. Hwang, and D.-K. Kim, "Numerical model for electrical explosion of copper wires in water," J. Appl. Phys. **120**(20), 203301 (2016).

[43]N. Shimomura, H. Akiyama, and S. Maeda, "Compact pulsed power generator by an inductive energy storage system with two-staged opening switches," IEEE Trans. Plasma Sci. **19**(6), 1220–1227 (1991).

[44]X. Li, Y. Chao, J. Wu, R. Han, H. Zhou, and A. Qiu, "Study of the shock waves characteristics generated by underwater electrical wire explosion," J. Appl. Phys. **118**(02), 023301 (2015).